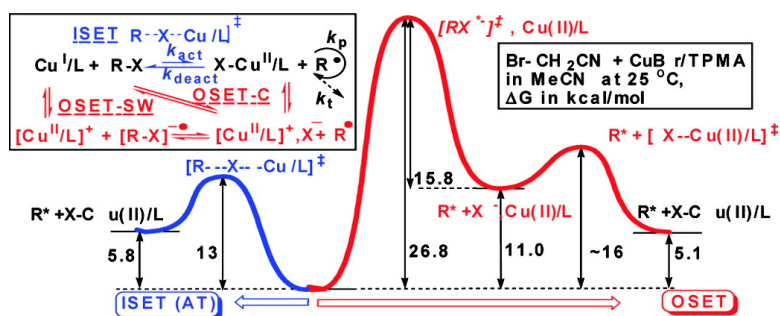Article

Ab Initio Evaluation of the Thermodynamic and Electrochemical Properties of Alkyl Halides and Radicals and Their Mechanistic Implications for Atom Transfer Radical Polymerization

Ching Yeh Lin, Michelle L. Coote, Armando Gennaro, and Krzysztof Matyjaszewski

More About This Article

Additional resources and features associated with this article are available within the HTML version:

- Supporting Information
- Access to high resolution figures
- Links to articles and content related to this article
- Copyright permission to reproduce figures and/or text from this article

View the Full Text HTML

Ab Initio Evaluation of the Thermodynamic and Electrochemical Properties of Alkyl Halides and Radicals and Their Mechanistic Implications for Atom Transfer Radical Polymerization

Ching Yeh Lin,[†] Michelle L. Coote,[*,†] Armando Gennaro,[*,‡] and
Krzysztof Matyjaszewski[*,§]

ARC Centre of Excellence for Free-Radical Chemistry and Biotechnology, Research School of Chemistry, Australian National University, Canberra ACT 0200, Australia, Dipartimento di Scienze Chimiche, Università di Padova, via Marzolo 1, 35131 Padova, Italy, Department of Chemistry, Carnegie Mellon University, 4400 Fifth Avenue, Pittsburgh, Pennsylvania 15213

Received May 23, 2008; E-mail: mcoote@rsc.anu.edu.au; armando.gennaro@unipd.it; km3b@andrew.cmu.edu

Abstract: High-level ab initio molecular orbital calculations are used to study the thermodynamics and electrochemistry relevant to the mechanism of atom transfer radical polymerization (ATRP). Homolytic bond dissociation energies (BDEs) and standard reduction potentials (SRPs) are reported for a series of alkyl halides (R−X; R = CH_2CN, $CH(CH_3)CN$, $C(CH_3)_2CN$, $CH_2COOC_2H_5$, $CH(CH_3)COOCH_3$, $C(CH_3)_2COOCH_3$, $C(CH_3)_2COOC_2H_5$, CH_2Ph, $CH(CH_3)Ph$, $CH(CH_3)Cl$, $CH(CH_3)OCOCH_3$, $CH(Ph)COOCH_3$, SO_2Ph, Ph; X = Cl, Br, I) both in the gas phase and in two common organic solvents, acetonitrile and dimethylformamide. The SRPs of the corresponding alkyl radicals, R•, are also examined. The computational results are in a very good agreement with the experimental data. For all alkyl halides examined, it is found that, in the solution phase, one-electron reduction results in the fragmentation of the R−X bond to the corresponding alkyl radical and halide anion; hence it may be concluded that a hypothetical outer-sphere electron transfer (OSET) in ATRP should occur via concerted dissociative electron transfer rather than a two-step process with radical anion intermediates. Both the homolytic and heterolytic reactions are favored by electron-withdrawing substituents and/or those that stabilize the product alkyl radical, which explains why monomers such as acrylonitrile and styrene require less active ATRP catalysts than vinyl chloride and vinyl acetate. The rate constant of the hypothetical OSET reaction between bromoacetonitrile and Cu^I/TPMA complex was estimated using Marcus theory for the electron-transfer processes. The estimated rate constant k_{OSET} = ~10^{-11} M^{-1} s^{-1} is significantly smaller than the experimentally measured activation rate constant (k_{ISET} = ~82 M^{-1} s^{-1} at 25 °C in acetonitrile) for the concerted atom transfer mechanism (inner-sphere electron transfer, ISET), implying that the ISET mechanism is preferred. For monomers bearing electron-withdrawing groups, the one-electron reduction of the propagating alkyl radical to the carbanion is thermodynamically and kinetically favored over the one-electron reduction of the corresponding alkyl halide unless the monomer bears strong radical-stabilizing groups. Thus, for monomers such as acrylates, catalysts favoring ISET over OSET are required in order to avoid chain-breaking side reactions.

Introduction

Controlled/living radical polymerization has progressively become a mature synthetic technique enabling the synthesis of many advanced materials with precisely controlled architectures.[1,2] Atom-transfer radical polymerization (ATRP) is one of most frequently used techniques due to the commercial availability of many initiators and catalysts.[3−6] However, the precise

mechanism of ATRP and the quantitative determination of chain-breaking reactions are still under extensive investigation.[7−12] This can be partially explained by the large variety of monomers, alkyl halides, and transition-metal complexes used for ATRP as well as the large range of experimental conditions (concentra-
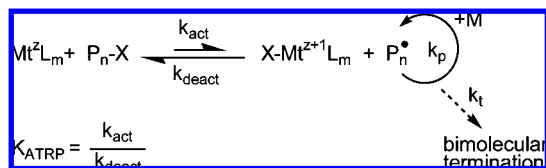

[†] Australian National University.
[‡] Università di Padova.
[§] Carnegie Mellon University.

(1) Matyjaszewski, K.; Gnanou, Y.; Leibler, L. *Macromolecular engineering*; Wiley VCH: Weinheim, 2007; Vol. 1.
(2) Braunecker, W. A.; Matyjaszewski, K. *Prog. Polym. Sci.* **2007**, *32*, 93–146.
(3) Matyjaszewski, K.; Xia, J. *Chem. Rev.* **2001**, *101*, 2921–2990.
(4) Kamigaito, M.; Ando, T.; Sawamoto, M. *Chem. Rev.* **2001**, *101*, 3689–3745.

(5) Matyjaszewski, K.; Spanswick, J. *Mater. Today* **2005**, *8*, 26–33.
(6) Tsarevsky, N. V.; Matyjaszewski, K. *Chem. Rev.* **2007**, *107*, 2270–2299.
(7) Matyjaszewski, K.; Davis, K.; Patten, T. E.; Wei, M. *Tetrahedron* **1997**, *53*, 15321–15329.
(8) Matyjaszewski, K. *Macromolecules* **1998**, *31*, 4710–4717.
(9) Matyjaszewski, K.; Paik, H.-j.; Shipp, D. A.; Isobe, Y.; Okamoto, Y. *Macromolecules* **2001**, *34*, 3127–3129.
(10) Singleton, D. A.; Nowlan, D. T.; Jahed, N.; Matyjaszewski, K. *Macromolecules* **2003**, *36*, 8609–8616.
(11) Haddleton, D. M.; Crossman, M. C.; Hunt, K. H.; Topping, C.; Waterson, C.; Suddaby, K. G. *Macromolecules* **1997**, *30*, 3992–3998.
(12) Harrisson, S.; Rourke, J. P.; Haddleton, D. M. *Chem. Commun.* **2002**, 1470–1471.

Scheme 1. ATRP Mechanism

Scheme 2. OSET vs ISET Processes in ATRP

Scheme 3. Oxidation and Reduction of Radicals to Carbocations and Carbanions via OSET

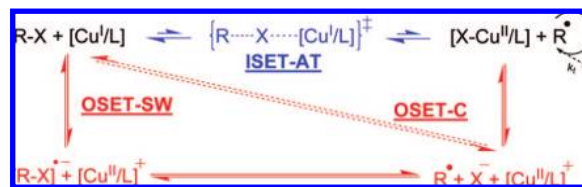

tions, addition modes, temperature, solvent, degree of homogeneity, etc.) under which it can be carried out.[13−16] In the present work, we use high-level ab initio molecular orbital calculations to study thermochemical and electrochemical aspects of the mechanism of ATRP with a view to aiding catalyst selection and design. The results are compared with recently determined ATRP equilibrium constants[17] and used to establish the reaction mechanism.
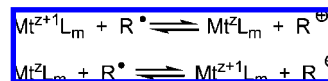
Scheme 1 presents the ATRP equilibrium in which the dormant alkyl halide (P_n-X) reacts with a transition-metal activator (Mt^zL_m) to reversibly form the propagating alkyl radical ($P_n^{\bullet}$) and transition-metal deactivator ($X-Mt^{z+1}L_m$).[18,19] Radicals propagate but also terminate,[20] and the relative rate of termination depends on the radical concentration, defined in turn by the equilibrium constant K_{ATRP}. This equilibrium depends on the reactivity of both the alkyl halides and the transition-metal complexes.[21−23]

Many transition-metal complexes have been successfully used in ATRP, including those of Cu, Ru, Fe, Mo, and Os.[24−30] Cu has been the most extensively studied, with over 50 ligands explored, generating ATRP catalysts with reactivities covering over 6 orders of magnitude.[21,29−34] In a similar way, the reactivities of alkyl halides and radicals are also dramatically affected by their structure as a result of their differing polar, steric, and resonance stabilization effects.[18,22]
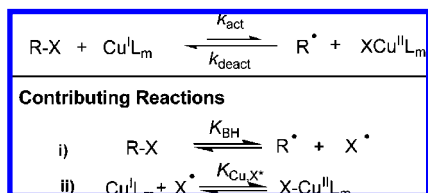
ATRP has been proposed to proceed by the concerted atom transfer mechanism, occurring via an inner-sphere electron-transfer (ISET) process.[3,8,35,36] However, alternatively, it could proceed by an outer-sphere electron-transfer (OSET) process in which the transition metal is oxidized to $Mt^{z+1}L_m$ and the alkyl halide is reduced. The OSET process for most alkyl halides takes place in solution in one step, forming the radical and halide anion by a concerted dissociative electron transfer (OSET-C).[37−39] There is also a possibility of a two-step process involving stable radical anion intermediates that subsequently cleave to a radical and a halide anion (OSET-SW).[40−42] Eventually, the halide anion migrates to $Mt^{z+1}L_m$ to form $X-Mt^{z+1}L_m$ species, i.e., exactly the same products as in ISET (see Scheme 2). We assigned no positive charge to both Cu^I and $X-Cu^{II}$ species in Scheme 2 and subsequent schemes, but this will change according to the structure of the ligand and counterion as well as the solvent and temperature.

The probability of the OSET process is directly correlated with the redox potentials of both the transition metal and alkyl halide. Redox processes can also involve the propagating radicals, which can be either reduced to carbanions or oxidized to carbocations (Scheme 3).[43,44] Both reactions will lead to chain-breaking processes by proton transfer or elimination, as already documented in the literature.[7,35,45−47] A knowledge of the preferred reaction mechanism, coupled with the relevant
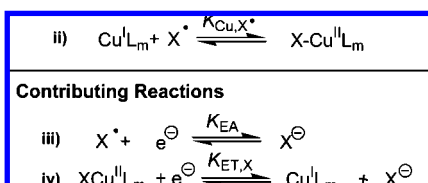
(13) Faucher, S.; Okrutny, P.; Zhu, S. *Ind. Eng. Chem. Res.* **2007**, *46*, 2726–2734.
(14) Chambard, G.; Klumperman, B.; German, A. L. *Macromolecules* **2000**, *33*, 4417–4421.
(15) Matyjaszewski, K.; Nakagawa, Y.; Jasieczek, C. B. *Macromolecules* **1998**, *31*, 1535–1541.
(16) Qiu, J.; Charleux, B.; Matyjaszewski, K. *Prog. Polym. Sci.* **2001**, *26*, 2083–2134.
(17) Tang, W.; Kwak, Y.; Braunecker, W.; Tsarevsky, N. V.; Coote, M. L.; Matyjaszewski, K. *J. Am. Chem. Soc.* **2008**, *130*, 10702–10713.
(18) Matyjaszewski, K.; Patten, T. E.; Xia, J. *J. Am. Chem. Soc.* **1997**, *119*, 674–680.
(19) Wang, J.-S.; Matyjaszewski, K. *J. Am. Chem. Soc.* **1995**, *117*, 5614–5615.
(20) Beuermann, S.; Buback, M. *Prog. Polym. Sci.* **2002**, *27*, 191–254.
(21) Tang, W.; Matyjaszewski, K. *Macromolecules* **2006**, *39*, 4953–4959.
(22) Tang, W.; Matyjaszewski, K. *Macromolecules* **2007**, *40*, 1858–1863.
(23) Tang, W.; Tsarevsky, N. V.; Matyjaszewski, K. *J. Am. Chem. Soc.* **2006**, *128*, 1598–1604.
(24) Poli, R. *Angew. Chem., Int. Ed.* **2006**, *45*, 5058–5070.
(25) Kato, M.; Kamigaito, M.; Sawamoto, M.; Higashimura, T. *Macromolecules* **1995**, *28*, 1721–1723.
(26) O'Reilly, R. K.; Gibson, V. C.; White, A. J. P.; Williams, D. J. *Polyhedron* **2004**, *23*, 2921–2928.
(27) Matyjaszewski, K.; Wei, M.; Xia, J.; McDermott, N. E. *Macromolecules* **1997**, *30*, 8161–8164.
(28) Braunecker, W. A.; Itami, Y.; Matyjaszewski, K. *Macromolecules* **2005**, 9402–9404.
(29) Xia, J.; Matyjaszewski, K. *Macromolecules* **1997**, *30*, 7697–7700.
(30) Xia, J.; Gaynor, S. G.; Matyjaszewski, K. *Macromolecules* **1998**, *31*, 5958–5959.
(31) Zhang, H.; Klumperman, B.; Ming, W.; Fischer, H.; van der Linde, R. *Macromolecules* **2001**, *34*, 6169–6173.
(32) Tang, H.; Arulsamy, N.; Radosz, M.; Shen, Y.; Tsarevsky, N. V.; Braunecker, W. A.; Tang, W.; Matyjaszewski, K. *J. Am. Chem. Soc.* **2006**, *128*, 16277–16285.
(33) Matyjaszewski, K.; Paik, H.-j.; Zhou, P.; Diamanti, S. J. *Macromolecules* **2001**, *34*, 5125–5131.
(34) Pintauer, T.; Matyjaszewski, K. *Coord. Chem. Rev.* **2005**, *249*, 1155–1184.

(35) Tsarevsky, N. V.; Braunecker, W. A.; Matyjaszewski, K. *J. Organomet. Chem.* **2007**, *692*, 3212–3222.
(36) Tsarevsky, N. V.; Braunecker, W. A.; Vacca, A.; Gans, P.; Matyjaszewski, K. *Macromol. Symp.* **2007**, *248*, 60–70.
(37) Isse, A. A.; Gennaro, A. *J. Phys. Chem. A* **2004**, *108*, 4180–4186.
(38) Cardinale, A.; Isse, A. A.; Gennaro, A.; Robert, M.; Saveant, J.-M. *J. Am. Chem. Soc.* **2002**, *124*, 13533–13539.
(39) Andrieux, C. P.; Merz, A.; Saveant, J. M.; Tomahogh, R. *J. Am. Chem. Soc.* **1984**, *106*, 1957–62.
(40) Percec, V.; Guliashvili, T.; Ladislaw, J. S.; Wistrand, A.; Stjerndahl, A.; Sienkowska, M. J.; Monteiro, M. J.; Sahoo, S. *J. Am. Chem. Soc.* **2006**, *128*, 14156–14165.
(41) Guliashvili, T.; Percec, V. *J. Polym. Sci., A: Polym. Chem.* **2007**, *45*, 1607–1618.
(42) Andrieux, C. P.; Gelis, L.; Medebielle, M.; Pinson, J.; Saveant, J. M. *J. Am. Chem. Soc.* **1990**, *112*, 3509–3520.
(43) Wayner, D. D. M.; Griller, D. *J. Am. Chem. Soc.* **1985**, *107*, 7764–7765.
(44) Lund, H.; Daasbjerg, K.; Lund, T.; Occhailini, D.; Pedersen, S. U. *Acta Chem. Scand.* **1997**, *51*, 135–144.
(45) Pietrasik, J.; Dong, H.; Matyjaszewski, K. *Macromolecules* **2006**, *39*, 6384–6390.
(46) Dong, H.; Tang, W.; Matyjaszewski, K. *Macromolecules* **2007**, *40*, 2974–2977.
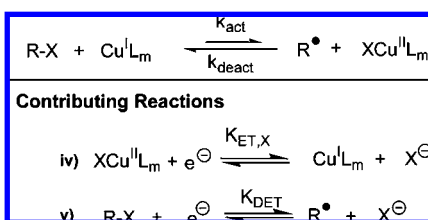(47) Matyjaszewski, K.; Jo, S. M.; Paik, H.-j.; Shipp, D. A. *Macromolecules* **1999**, *32*, 6431–6438.

Scheme 4. Atom Transfer as a Combination of C−X Bond Homolysis of an Alkyl Halide (RX) and Cu^{II}−X Bond Formation (Halogenophilicity)

$$R\text{-}X \;+\; Cu^I L_m \;\underset{k_{deact}}{\overset{k_{act}}{\rightleftharpoons}}\; R^\bullet \;+\; XCu^{II}L_m$$

Contributing Reactions

$$i) \qquad R\text{-}X \;\overset{K_{BH}}{\rightleftharpoons}\; R^\bullet \;+\; X^\bullet$$

$$ii) \quad Cu^I L_m + X^\bullet \;\overset{K_{Cu,X^\bullet}}{\rightleftharpoons}\; X\text{-}Cu^{II}L_m$$

Scheme 5. Halogenophilicity as a Combination of Electron Affinity of Halogen Atoms and Dissociative Reduction of Cu^{II}−X Species

$$ii) \quad Cu^I L_m + X^\bullet \;\overset{K_{Cu,X^\bullet}}{\rightleftharpoons}\; X\text{-}Cu^{II}L_m$$

Contributing Reactions

$$iii) \quad X^\bullet + e^\ominus \;\overset{K_{EA}}{\rightleftharpoons}\; X^\ominus$$

$$iv) \quad XCu^{II}L_m + e^\ominus \;\overset{K_{ET,X}}{\rightleftharpoons}\; Cu^I L_m \;+\; X^\ominus$$

Scheme 6. Atom Transfer as a Combination of Dissociative Electron Transfer and Dissociative Reduction of Deactivator

$$R\text{-}X \;+\; Cu^I L_m \;\underset{k_{deact}}{\overset{k_{act}}{\rightleftharpoons}}\; R^\bullet \;+\; XCu^{II}L_m$$

Contributing Reactions

$$iv) \quad XCu^{II}L_m + e^\ominus \;\overset{K_{ET,X}}{\rightleftharpoons}\; Cu^I L_m \;+\; X^\ominus$$

$$v) \quad R\text{-}X \;+\; e^\ominus \;\overset{K_{DET}}{\rightleftharpoons}\; R^\bullet \;+\; X^\ominus$$

redox potentials of the various species, is important as it can be used to guide catalyst selection so as to optimize the process and avoid such chain-breaking side reactions.

The overall atom transfer equilibrium can be viewed as a hypothetical combination of two formal simple reversible reactions: (i) C−X bond homolysis (K_{BH}) and (ii) X−Cu^{II}L$_m$ bond homolysis, as shown in Scheme 4. In that case, $K_{ATRP} = K_{BH}K_{Cu,X}$. The second reaction depends on the catalyst and will not be analyzed in detail in this paper. The affinity of the Cu^{I}L$_m$ complex for the halogen atom, i.e., halogenophilicity, is nearly as large as the affinity of carbon-based radicals for halogens. The difference between free energies of these two homolytic bond cleavage processes defines the values of the ATRP equilibrium constant. It is worth noting that halogenophilicity is quite different from halidophilicity, i.e., the affinity of Cu(II) species for the halide anion, which is reversibly related to heterolytic cleavage of X−Cu^{II}L$_m$.[36]

The reaction representing halogenophilicity can be further split into two formally contributing reactions: (iii) reduction of a halogen atom to a halide ion (electron affinity of X$^\bullet$, K_{EA}) and (iv) dissociative reduction of X−Cu^{II}L$_m$ species to form the halide anion and Cu^{I}L$_m$ species, as shown in Scheme 5. In that case, $K_{Cu,X^\bullet} = K_{EA}/K_{ET,X}$.

Alternatively, the ATRP equilibrium can be formally represented as a combination of two electron-transfer processes: (iv) dissociative reduction of X−Cu^{II}L$_m$ species to form halide anion and Cu^{I}L$_m$ species and (v) dissociative electron transfer (DET) of alkyl halide to a radical and a halide anion, as illustrated in Scheme 6. In that case, $K_{ATRP} = K_{DET}/K_{ET,X}$.

Schemes 3–6 show how important it is to know both the thermodynamic and electrochemical properties of alkyl halides, radicals, and transition-metal complexes. The redox potentials of ATRP catalysts have been determined for several

systems.[26,48−53] Regrettably, the experimental values of the redox potentials of alkyl halides and radicals are very limited. Fortunately, recent progress in computational chemistry provides access to reliable electrochemical data for organic molecules in solution, and this is particularly useful in situations where complex chemical equilibria are known to hamper experimental measurements.

In this paper, the thermodynamic and electrochemical properties of alkyl halides used as ATRP initiators (often with structures mimicking dormant chain ends) are determined with state-of-the-art precision. In addition, the redox properties of the radicals have been computed. The results allow us to better understand the ATRP mechanism and to guide catalyst selection for the optimal ATRP process, in terms of proper polymerization rate and also suppression of catastrophic chain-breaking reactions. As part of this work, we analyze the mechanism of ATRP, comparing the ISET and OSET processes for the case study of bromoacetonitrile with a CuI/TPMA catalyst. We also make a more general comparison of two alternative pathways for the OSET process itself, a concerted DET (OSET-C) and a two-step process (OSET-SW). The latter has been suggested as a preferred pathway for reactions with Cu(0) with a proposed single-electron-transfer (SET) mechanism.[40] The computational results show that hypothetical OSET for alkyl halides relevant to ATRP should preferentially occur by concerted DET, in agreement with available experimental data,[37] though for our case study at least, the ISET process is kinetically preferred over any OSET process.

Theoretical Procedures

Standard ab initio and density functional theory calculations were performed in GAUSSIAN 03.[54] Calculations were performed at a high level of theory, chosen on the basis of recent assessment studies for alkyl halide homolytic bond dissociation energies (BDEs)[55,56] and for the one-electron oxidation and reduction potentials of closed- and open-shell species in organic solvents.[57,58] Further evaluations of the accuracy of the present calculations are carried out below and in the Supporting Information, where a comparison of the present high-level data with those from earlier DFT studies[41,59,60] is also provided. We find that, for the alkyl chlorides and bromides, the current procedures are capable of reproducing BDEs and standard reduction potentials (SRPs) to within chemical accuracy (ca. 1 kcal mol^{-1}); for the heavier iodides, the errors may be somewhat larger due to, for example, the greater importance of

(48) Qiu, J.; Matyjaszewski, K.; Thouin, L.; Amatore, C. *Macromol. Chem. Phys.* **2000**, *201*, 1625–1631.
(49) Matyjaszewski, K.; Goebelt, B.; Paik, H.-j.; Horwitz, C. P. *Macromolecules* **2001**, *34*, 430–440.
(50) Ando, T.; Kamigaito, M.; Sawamoto, M. *Macromolecules* **2000**, *33*, 5825–5829.
(51) Coullerez, G.; Carlmark, A.; Malmstroem, E.; Jonsson, M. *J. Phys. Chem. A* **2004**, *108*, 7129–7131.
(52) Braunecker, W. A.; Brown, W. C.; Morelli, B. C.; Tang, W.; Poli, R.; Matyjaszewski, K. *Macromolecules* **2007**, *40*, 8576–8585.
(53) Coullerez, G.; Malmstroem, E.; Jonsson, M. *J. Phys. Chem. A* **2006**, *110*, 10355–10360.
(54) Frisch, M. J., et al. *Gaussian 03*, Revision B.03; Gaussian, Inc.: Pittsburgh, PA, 2003.
(55) Izgorodina, E. I.; Brittain, D. R. B.; Hodgson, J. L.; Krenske, E. H.; Lin, C. Y.; Namazian, M.; Coote, M. L. *J. Phys. Chem. A* **2007**, *111*, 10754–10768.
(56) Izgorodina, E. I.; Coote, M. L.; Radom, L. *J. Phys. Chem. A* **2005**, *109*, 7558–7566.
(57) Namazian, M.; Coote, M. L. *J. Phys. Chem. A* **2007**, *111*, 7227–7232.
(58) Hodgson, J. L.; Namazian, M.; Bottle, S. E.; Coote, M. L. *J. Phys. Chem. A* **2007**, *111*, 13595–13605.
(59) Matyjaszewski, K.; Poli, R. *Macromolecules* **2005**, *38*, 8093–8100.
(60) Gillies, M. B.; Matyjaszewski, K.; Norrby, P.-O.; Pintauer, T.; Poli, R.; Richard, P. *Macromolecules* **2003**, *36*, 8551–8559.

core correlation effects. Thus, we include these latter data for the purposes of qualitative comparison only.

For the alkyl chlorides, bromides, and associated species, geometries were optimized at the B3LYP/6-31+G(d) level of theory, and frequencies were also calculated at this level and scaled via the appropriate scale factors.[61] B3-LYP/6-31G(d) has been shown to deliver accurate geometries and frequencies for the stable molecules in radical reactions;[62] in the present systems we include an additional set of diffuse functions so as to facilitate a better description of the weakly bound electrons in the anions. Improved energies were calculated using G3(MP2)-RAD(+). G3(MP2)-RAD is a high-level composite method that approximates (UR)CCSD(T) energies with a large triple-ζ basis set via additivity corrections at the R(O)MP2 level of theory.[63] Spin-orbit corrections for atoms are included as part of this method. In the "+" variant of this method, calculations with the 6-31G(d) basis set are replaced with corresponding calculations with the 6-31+G(d) basis set, so as to allow for a better treatment of anionic species. In the present work we also use UCCSD(T) energies in place of (UR)CCSD(T) energies for the open-shell species in order to address convergence problems experienced with the latter method for some of the radical anions. For the heavier iodine atom, all calculations with the 6-31+G(d) basis set were performed with the effective core potential LACVP+*; calculations with the G3MP2large basis set were performed using the all-electron basis set 6-311+G(3df,2p).

For all species, gas-phase free energies were calculated using the B3LYP/6-31+G(d) geometries and frequencies and G3(MP2)-RAD(+) total energies, using the standard textbook formulas based on the statistical thermodynamics of an ideal gas under the rigid rotor/harmonic oscillator approximation. For the BDE calculations, we then corrected all low-frequency torsional modes using the more accurate hindered rotor model. For this purpose we used the 60° resolution full torsional eigenvalue summation (TES) model, as our recent assessment study of 644 rotations in 104 organic molecules showed that this resolution was sufficient to reproduce the results obtained at the more accurate 10° resolution to within a factor of 1.08.[64]

The free energies of solvation for the studied molecules in acetonitrile and dimethylformamide (DMF) were calculated using the conductor-like polarizable continuum model (CPCM)[65] at the HF/6-31+G(d) level of theory. The radii of the united atom topological model, optimized for the Hartree−Fock level of theory (UAHF), have been chosen for the determination of solvation energies as recommended.[54] For acetonitrile, the rest of the parameters of the CPCM model, such as $f(\alpha)$ were kept as their default values in GAUSSIAN.[54] For DMF, the solvent parameters were not available as default values in GAUSSIAN. Instead, calculations were carried out using dichloroethane as the nominal solvent, as its molecular volume is similar to that of DMF, but with the UAHF radius (2.647 Å), dielectric constant (36.71), and numerical density (0.00777795 Å^{-3}) adjusted to the correct DMF values.[66] For the solvation energy calculations, unless noted otherwise, all geometries of the studied species were optimized fully in the presence of solvent using HF/6-31+G(d). Single-point solvation energy calculations were then performed at the R(O)HF/6-31+G(d) level of theory. All solvation energy calculations were performed using the SCFVAC keyword in Gaussian so that the solvation energy, rather than the total free energy in the solvent, could be extracted and combined with higher-level calculations of the free energy in the gas phase.

The combination of CPCM with R(O)HF/6-31+G(d) was found to perform well in our recent study of the one-electron reduction potentials of quinones in acetonitrile, leading to predicted values within 0.07 V of experiment.[57] Where comparison is possible in the present work, the calculated and experimental SRPs show a similar level of deviation (0.05 V, see Supporting Information). When calculating the potential energy surfaces for the dissociation of RX$^{\bullet-}$ into R$^{\bullet}$ and X^{-}, we also performed calculations using a more sophisticated solvation model, COSMO-RS.[67] This method describes the interactions in a fluid as local contact interactions of molecular surfaces instead of making mean field assumptions, as in CPCM. We found that the use of this more advanced method affected the results by less than 1 kcal mol^{-1}, and hence its use in calculating the SRPs of the entire test set was not justified.

Standard one-electron reduction potentials (SRPs) for the alkyl halides (RX) and alkyl radicals (R$^{\bullet}$) were calculated as follows. For each half-reaction studied (i.e., X$_{aq}$ + e$^{-}_{g}$ → X$^{-}_{aq}$, R$^{\bullet}_{aq}$ + e$^{-}_{g}$ → R$^{-}_{aq}$, RX$_{aq}$ + e$^{-}_{g}$ → RX$^{\bullet-}_{aq}$, and RX$_{aq}$ + e$^{-}_{g}$ → R$^{\bullet}_{aq}$ + X$^{-}_{aq}$), the Gibbs free energy of reaction in the gas-phase, $\Delta G°$(g), and the Gibbs free energies of solvation, $\Delta G°$(solv), of the reactant and product(s) were first calculated using the procedures described above. Using a simple thermodynamic cycle, it was then possible to calculate the solution-phase Gibbs free energy of reaction, $\Delta G°$(soln), via eq 1.

$$\Delta G°(\text{soln}) = \Delta G°(\text{g}) + \Delta\Delta G°(\text{solv}) + \Delta m RT \ln(24.46) \quad (1)$$

This includes a correction term, $\Delta m\, RT \ln(24.46)$, where Δm is the change in number of moles of solvated species on reaction, in order to take in account that $\Delta G°$(solv) is computed for the passage from 1 mol L^{-1}(g) to 1 mol L^{-1}(soln). For the majority of reactions studied herein, $\Delta m = 0$; however, for dissociative electron transfer (RX$_{aq}$ + e$^{-}_{g}$ → R$^{\bullet}_{aq}$ + X$^{-}_{aq}$), $\Delta m = 1$. The resulting value of $\Delta G°$(soln) is related to the absolute formal reduction potential, $E°$, according to eq 2,

$$E° = -\Delta G°(\text{soln})/nF \quad (2)$$

where n is the number of electrons transferred ($n = 1$ in this case) and F is the Faraday constant (96 485.338 C mol^{-1}). For the free electron, we have followed the electron convention, as used in the "Fermi−Dirac electron energetics".[68] Finally, the calculated absolute reduction potentials were converted to SRPs relative to the aqueous saturated calomel electrode (SCE) by subtracting 4.388 and 4.307 V for acetonitrile and DMF, respectively. These values are obtained by adding the SCE potential (0.241 V) to the absolute aqueous standard hydrogen potential (4.24 V) and subtracting the appropriate interliquid potential for the respective solvents (0.093 V for acetonitrile and 0.174 V for DMF).[69]

Results

Homolytic alkyl halide bond dissociation energies (eq i in Scheme 4) for a series of alkyl halides at 298.15 K, both in the gas phase and in two common organic solvents (acetonitrile and DMF), are provided in Table 1. Our test set of alkyl halides is shown in Figure 1, and includes common ATRP initiators as well as species that mimic the dormant chain ends in the polymerization of various common monomers such as acrylonitrile (AN), methyl acrylate (MA), methyl methacrylate (MMA), styrene (STY), vinyl chloride (VC), and vinyl acetate (VAc). We also included phenyl halides in our test set as an example of a species that is not active in ATRP. Calculations were performed for the chlorides, bromides, and iodides; however, as noted above, for the iodides we do not expect the results to be of comparable accuracy to those for the smaller

(61) Scott, A. P.; Radom, L. *J. Phys. Chem.* **1996**, *100*, 16502–16513.
(62) Coote, M. L. *J. Phys. Chem. A* **2004**, *108*, 3865–3872.
(63) Henry, D. J.; Sullivan, M. B.; Radom, L. *J. Chem. Phys.* **2003**, *118*, 4849–4860.
(64) Lin, C. Y.; Izgorodina, E. I.; Coote, M. L. *J. Phys. Chem. A* **2008**, *112*, 1956–1964.
(65) Cossi, M.; Rega, N.; Scalmani, G.; Barone, V. *J. Comput. Chem.* **2003**, *24*, 669.
(66) Böes, E. S.; Livotto, P. R.; Stassen, H. *Chem. Phys.* **2006**, *331*, 142–158.
(67) Eckert, F.; Klamt, A. *AIChE J.* **2002**, *48*, 369.
(68) Bartmess, J. E. *J. Phys. Chem.* **1994**, *98*, 6420.
(69) Izutsu, K. *Electrochemistry in Nonaqueous Solutions*; Wiley: New York, 2001.

Table 1. Enthalpy, Entropy, and Free Energy (298.15 K; kcal mol^{-1})^a for Homolytic Cleavage of Alkyl Halides, R–X → R$^{\bullet}$ + X$^{\bullet}$, in the Gas and Solution Phases

halide	ΔH, gas phase	$-T\Delta S$, gas phase	ΔG gas phase	acetonitrile	DMF
MeCN–Cl	71.58	−8.62	62.96	63.49	64.48
AN–Cl	72.16	−9.27	62.89	61.59	62.30
IBN–Cl	72.53	−9.25	63.27	62.08	62.90
EAc–Cl	76.68	−10.01	66.68	66.06	66.76
MA–Cl	75.70	−8.44	67.26	66.33	66.97
MMA–Cl	75.32	−8.81	66.51	65.58	66.36
EtiB–Cl	75.47	−10.06	65.41	64.37	65.12
PhCH$_2$–Cl	73.90	−8.25	65.65	65.78	66.49
STY–Cl	75.34	−10.08	65.26	64.89	65.52
VC–Cl	80.39	−9.68	70.70	70.36	71.08
VAc–Cl	84.27	−10.37	73.90	73.27	73.90
MPA–Cl	67.82	−8.15	59.67	58.66	58.99
PhSO$_2$–Cl	67.12	−9.56	57.56	57.75	58.69
Ph–Cl	99.91	−9.53	90.38	89.34	89.99
MeCN–Br	58.86	−8.52	50.35	50.64	51.61
AN–Br	58.92	−9.18	49.74	48.20	48.86
IBN–Br	58.80	−9.17	49.62	48.15	48.93
EAc–Br	63.95	−8.31	55.63	54.76	55.41
MA–Br	62.84	−9.01	53.83	52.59	53.16
MMA–Br	61.75	−8.92	52.83	51.61	52.33
EtiB–Br	61.91	−10.20	51.71	50.36	51.06
PhCH$_2$–Br	61.12	−8.31	52.81	52.65	53.30
STY–Br	61.58	−8.48	53.10	52.50	53.05
VC–Br	66.19	−9.58	56.61	55.96	56.65
VAc–Br	69.91	−10.31	59.60	58.69	59.25
MPA–Br	54.68	−8.13	46.55	45.10	45.42
PhSO$_2$–Br	53.76	−9.40	44.36	44.19	45.06
Ph–Br	85.65	−9.40	76.25	74.96	75.57
MeCN–I	47.71	−8.37	39.34	39.49	40.46
AN–I	47.07	−9.04	38.03	36.32	37.01
IBN–I	46.44	−9.00	37.44	35.85	36.67
EAc–I	53.03	−8.27	44.75	43.53	44.17
MA–I	51.14	−8.56	42.59	41.01	41.59
MMA–I	49.57	−8.85	40.72	39.25	40.00
EtiB–I	49.76	−9.95	39.80	38.19	38.91
PhCH$_2$–I	49.59	−8.21	41.38	40.81	41.46
STY–I	49.71	−9.84	39.87	38.89	39.45
VC–I	52.96	−9.38	43.58	42.71	43.41
VAc–I	56.25	−10.18	46.08	44.78	45.39
MPA–I	44.06	−8.17	35.89	33.84	34.21
PhSO$_2$–I	41.70	−9.18	32.52	32.24	33.09
Ph–I	73.25	−9.20	64.05	62.58	63.20

^{a} Calculated at the G3(MP2)-RAD(+)//B3LYP/6-31+G(d) level of theory using the hindered rotor model. Solvation effects calculated using the CPCM continuum model of solvation at the HF/6-31+G(d) level of theory and using UAHF radii.

chlorides and bromides, and the results are included for qualitative purposes only. The B3LYP/6-31+G(d) optimized geometries of all species are provided in the Supporting Information.

"Heterolytic" alkyl halide BDEs for the alkyl halides at 298.15 K, both in the gas phase and in acetonitrile and DMF, are provided in Table 2. As in the earlier work of Guliashvili and Percec,[41] the heterolytic BDE was defined as the energy change of the half-reaction in which the one-electron reduction of the alkyl halide results in dissociation to the corresponding alkyl radical and halide anion (eq v in Scheme 6). It should be noted that the free energy change for this reaction is simply the sum of the free energy changes associated with the homolytic dissociation and the reduction of the halogen to the corresponding halide anion. In the present work we have considered not only the enthalpy of reaction v in Scheme 6, but also the entropy and overall free energy change, both in the gas and solution phases, thereby allowing us better to predict the behavior of
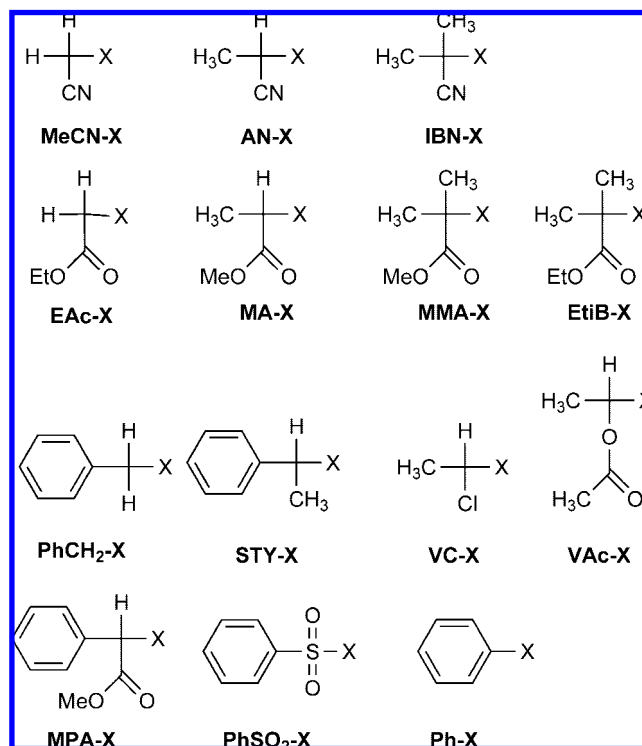
Figure 1. Species studied (X = Cl, Br, I, or unpaired electron).

the alkyl halides in a practical experimental setting. Results for the alkyl iodides are included in Table 2, though, as noted above, these results may be subject to larger errors than those for the smaller chlorides and bromides.

The gas-phase electron affinities and one-electron standard reduction potentials of the alkyl halides are shown in Table 3; those for the alkyl and halogen radicals are shown in Table 4. The SRPs were calculated for reductions in both acetonitrile and DMF and are quoted against the relevant value of the aqueous SCE. It should be noted that, following standard conventions, the electron affinity (EA) is defined as the negative of the *enthalpy* of the one-electron reduction reaction at 0 K; the SRP is a function of the negative of the *free energy* of the reduction reaction. Thus, in each case, the more positive (or less negative) the value, the more easily the species is reduced. This is in contrast to the enthalpies and free energies of Tables 1 and 2, where the most favorable reactions have the most exoergic values.

We considered two different cases for the one-electron reduction of the alkyl halides and their subsequent dissociation: (a) the adiabatic EA and associated reduction potential, in which the resulting alkyl halide "radical anion" is fully optimized, and (b) the complete dissociation of the alkyl halide into the alkyl radical and halide anion via reaction v above. The B3LYP/6-31+G(d) optimized geometries of the alkyl halide "radical anions" in the gas phase are shown in Figure 2. As we will discuss later, it is clear from this figure that the alkyl halide "radical anions" undergo substantial rearrangement to form complexes between the corresponding alkyl radicals and halide anions, so we can speak of radical and anion pairs rather than radical anions. In the solution phase, the radical−halide distance was greater to the extent that, in the majority of cases, the complexes completely dissociated and stable bound structures could not be found. Even where stable structures could be found (i.e., for MeCN−X, AN−X, IBN−X, PhSO$_2$−X, and VC−X),

Table 2. Enthalpy, Entropy, and Free Energy (298.15 K; kcal mol^{-1})^a for Heterolytic Cleavage of Alkyl Halides, R−X + e$^-$ → R$^•$ + X$^-$, in the Gas and Solution Phases

				ΔG	
halide	ΔH, gas-phase	$-T\Delta S$, gas-phase	gas phase	acetonitrile	DMF
MeCN−Cl	−15.03	−6.59	−21.62	−87.97	−87.47
AN−Cl	−14.45	−7.24	−21.69	−89.87	−89.65
IBN−Cl	−14.08	−7.22	−21.30	−89.39	−89.06
EAc−Cl	−9.92	−7.97	−17.90	−85.40	−85.19
MA−Cl	−10.90	−6.41	−17.32	−85.13	−84.98
MMA−Cl	−11.29	−6.78	−18.07	−85.89	−85.60
EtiB−Cl	−11.14	−8.03	−19.17	−87.09	−86.83
PhCH$_2$−Cl	−12.71	−6.21	−18.92	−85.69	−85.47
STY−Cl	−11.26	−8.05	−19.32	−86.57	−86.43
VC−Cl	−6.22	−7.65	−13.87	−81.11	−80.88
VAc−Cl	−2.34	−8.34	−10.68	−78.19	−78.05
MPA−Cl	−18.79	−6.12	−24.90	−92.81	−92.97
PhSO$_2$−Cl	−19.48	−7.53	−27.01	−93.72	−93.27
Ph−Cl	13.30	−7.50	5.80	−62.12	−61.96
MeCN−Br	−21.73	−6.48	−28.21	−90.66	−90.22
AN−Br	−21.67	−7.15	−28.82	−93.10	−92.97
IBN−Br	−21.80	−7.14	−28.94	−93.15	−92.90
EAc−Br	−16.64	−6.28	−22.93	−86.54	−86.42
MA−Br	−17.75	−6.98	−24.73	−88.71	−88.67
MMA−Br	−18.84	−6.89	−25.73	−89.69	−89.50
EtiB−Br	−18.68	−8.17	−26.85	−90.94	−90.77
PhCH$_2$−Br	−19.47	−6.28	−25.75	−88.65	−88.53
STY−Br	−19.01	−6.45	−25.47	−88.80	−88.78
VC−Br	−14.40	−7.55	−21.95	−85.34	−85.18
VAc−Br	−10.69	−8.28	−18.96	−82.62	−82.59
MPA−Br	−25.91	−6.10	−32.01	−96.20	−96.41
PhSO$_2$−Br	−26.83	−7.37	−34.20	−97.11	−96.77
Ph−Br	5.06	−7.37	−2.31	−66.34	−66.26
MeCN−I	−24.53	−6.34	−30.87	−86.23	−85.91
AN−I	−25.16	−7.01	−32.17	−89.41	−89.37
IBN−I	−25.80	−6.97	−32.77	−89.88	−89.71
EAc−I	−19.21	−6.24	−25.46	−82.20	−82.21
MA−I	−21.09	−6.53	−27.62	−84.71	−84.78
MMA−I	−22.67	−6.82	−29.49	−86.48	−86.38
EtiB−I	−22.48	−7.92	−30.40	−87.54	−87.47
PhCH$_2$−I	−22.65	−6.18	−28.83	−84.91	−84.91
STY−I	−22.52	−7.81	−30.33	−86.84	−86.93
VC−I	−19.27	−7.35	−26.62	−83.02	−82.97
VAc−I	−15.98	−8.15	−24.13	−80.95	−80.99
MPA−I	−28.18	−6.14	−34.32	−91.88	−92.16
PhSO$_2$−I	−30.54	−7.15	−37.69	−93.48	−93.28
Ph−I	1.02	−7.17	−6.16	−63.14	−63.17

^{a} Calculated at the G3(MP2)-RAD(+)//B3LYP/6-31+G(d) level of theory using the hindered rotor model. Solvation effects calculated using the CPCM model at the HF/6-31+G(d) level of theory with UAHF radii.

Table 3. Gas-Phase Electron Affinity (EA, eV) at 0 K and Standard Reduction Potential (SRP, V vs SCE) in Acetonitrile and DMF at 298.15 K for the Adiabatic and Dissociative Reductions of Alkyl Halides^a

	EA (eV), gas-phase		SRP (V vs SCE) in acetonitrile		SRP (V vs SCE) in DMF	
halide	adiab	dissoc	adiab	dissoc	adiab	dissoc
MeCN−Cl	1.03	0.47	−0.91	−0.57	−0.85	−0.51
AN−Cl	1.15	0.46	−0.82	−0.46	−0.76	−0.39
IBN−Cl	1.15	0.46	−0.86	−0.46	−0.81	−0.39
EAc−Cl	0.65	0.26	−1.18	−0.74	−1.12	−0.67
MA−Cl	0.75	0.30	−1.04	−0.65	−0.98	−0.58
MMA−Cl	0.82	0.32	−1.04	−0.56	−1.00	−0.50
EtiB−Cl	0.81	0.31	−1.05	−0.58	−1.00	−0.51
PhCH$_2$−Cl	0.81	0.37	−1.05	−0.67	−1.00	−0.60
STY−Cl	0.73	0.33	−1.04	−0.65	−0.99	−0.57
VC−Cl	0.55	0.10	−1.26	−0.85	−1.21	−0.78
VAc−Cl	0.27	−0.06	−1.43	−0.99	−1.38	−0.91
MPA−Cl	1.04	0.67	−0.88	−0.36	−0.82	−0.27
PhSO$_2$−Cl	1.56	0.72	−0.62	−0.32	−0.57	−0.26
Ph−Cl	−0.49	−0.71	−2.12	−1.69	−2.03	−1.62
MeCN−Br	1.28	0.77	−0.78	−0.46	−0.71	−0.39
AN−Br	1.41	0.78	−0.67	−0.32	−0.61	−0.25
IBN−Br	1.42	0.80	−0.68	−0.30	−0.63	−0.23
EAc−Br	0.92	0.55	−1.03	−0.62	−0.96	−0.54
MA−Br	0.95	0.61	−0.91	−0.51	−0.85	−0.43
MMA−Br	1.10	0.66	−0.85	−0.40	−0.80	−0.33
EtiB−Br	1.08	0.65	−0.86	−0.42	−0.81	−0.35
PhCH$_2$−Br	1.06	0.68	−0.90	−0.55	−0.84	−0.47
STY−Br	1.02	0.66	−0.86	−0.50	−0.81	−0.42
VC−Br	0.87	0.47	−1.05	−0.67	−1.00	−0.60
VAc−Br	0.61	0.31	−1.21	−0.80	−1.16	−0.72
MPA−Br	1.32	0.99	−0.69	−0.20	−0.63	−0.11
PhSO$_2$−Br	1.83	1.05	−0.45	−0.18	−0.39	−0.11
Ph−Br	−0.11	−0.34	−1.91	−1.51	−1.83	−1.43
MeCN−I	1.39	0.90	−0.90	−0.65	−0.83	−0.58
AN−I	1.53	0.94	−0.78	−0.48	−0.72	−0.40
IBN−I	1.55	0.98	−0.76	−0.44	−0.71	−0.37
EAc−I	1.04	0.67	−1.14	−0.81	−1.07	−0.73
MA−I	1.14	0.76	−0.98	−0.68	−0.91	−0.59
MMA−I	1.23	0.83	−0.93	−0.55	−0.88	−0.47
EtiB−I	1.22	0.81	−0.93	−0.57	−0.87	−0.49
PhCH$_2$−I	1.18	0.83	−0.99	−0.71	−0.93	−0.63
STY−I	1.18	0.83	−0.93	−0.64	−0.87	−0.55
VC−I	1.06	0.69	−1.10	−0.77	−1.04	−0.69
VAc−I	0.82	0.55	−1.24	−0.87	−1.19	−0.79
MPA−I	1.43	1.09	−0.78	−0.39	−0.72	−0.30
PhSO$_2$−I	1.98	1.21	−0.47	−0.34	−0.42	−0.26
Ph−I	0.13	−0.16	−1.93	−1.65	−1.85	−1.57

^{a} Calculated at the G3(MP2)-RAD(+)//B3LYP/6-31+G(d) level of theory using the harmonic oscillator approximation. Solvation effects calculated using the CPCM model at the HF/6-31+G(d) level of theory with UAHF radii. The EA is defined as $-\Delta H$ for the reduction reaction. In the adiabatic (adiab) case, the geometry is reoptimized, resulting in a weak complex between the alkyl radical and halide ion; in the dissociative (dissoc) case, the complete heterolytic dissociation, RX + e$^-$ → R$^•$ + X$^-$, is considered.

the alkyl halide distances exceeded 4 Å and the free energies of the complexes were higher than those of the fully dissociated species. For the solution-phase SRPs, we therefore calculated the "adiabatic" values using the optimized gas-phase geometries of the halide radical anions.

Discussion

Homolytic BDEs. Examining first the R−X homolytic BDEs (Table 1), we note that, as expected, the alkyl chloride BDEs are higher than the corresponding alkyl bromide BDEs, which are in turn higher than the alkyl iodide BDEs. This presumably stems from a combination of poorer overlap and decreasing ionic character in the order Cl > Br > I. Poor overlap combined with the high stability of the resulting sulfur-centered radical also results in PhSO$_2$−X having the lowest BDEs within each series of halides and explains their efficiency as ATRP initiators. Within each series of alkyl halides, the trends in the gas-phase

enthalpies largely follow those expected on the basis of the radical stabilization energies (RSEs) of the product alkyl radicals, as obtained from R−H bond homolysis. Thus, of the alkyl halides, MPA−X has the lowest BDE due to the high stability of the captodatively stabilized MPA radical; at the other extreme, the phenyl radical is the least stable, and Ph−X accordingly has the highest BDE. This latter result explains why Ph−X is not an active ATRP initiator. We also note that VAc−X and VC−X have relatively high BDEs, consistent with the relatively low stabilization energies of the VAc and VC radicals, while STY−X and AN−X have much lower BDEs, consistent with the higher stabilities of their corresponding alkyl radicals (the RSEs of VAc, VC, STY, and AN radicals are 5.8,

Table 4. Gas-Phase Electron Affinity (EA, eV) at 0 K and Standard Reduction Potential (SRP, V vs SCE) in Acetonitrile and DMF for the Alkyl Radicals and Halogen Atoms at 298.15 K[a]

species	EA (eV), gas phase	SRP (V vs SCE)	
		acetonitrile	DMF
Cl	3.68	2.18	2.28
Br	3.42	1.74	1.84
I	3.06	1.06	1.17
MeCN	1.58	−0.42	−0.32
AN	1.26	−0.86	−0.76
IBN	1.11	−1.08	−0.99
EAc	1.67	−0.46	−0.39
MA	1.43	−0.71	−0.63
MMA	1.29	−0.98	−0.91
EtiB	1.30	−1.04	−0.96
PhCH$_2$	0.94	−1.50	−1.43
STY	0.85	−1.61	−1.53
VC	0.57	−1.28	−1.24
VAc	0.36	−1.64	−1.57
MPA	2.04	−0.41	−0.33
PhSO$_2$	2.72	0.36	0.44
Ph	1.21	−0.82	−0.74

[a] Calculated at the G3(MP2)-RAD(+)//B3LYP/6-31+G(d) level of theory. Solvation effects calculated using the CPCM model at the HF/6-31+G(d) level of theory with UAHF radii. The EA is defined as $-\Delta H$ for the reduction reaction.

6.5, 16.3, and 11.3 kcal mol^{-1}, respectively).[70] This is consistent with the experimental observation that styrene and acrylonitrile require less active ATRP catalysts than vinyl chloride and vinyl acetate.

However, there are some minor exceptions to this general trend. In particular, the STY−X and PhCH$_2$−X BDEs are not as low as might have been expected on the basis of radical stability considerations. The RSE of the STY radical is 5 kcal mol^{-1} greater than that of the AN radical, yet its corresponding R−X BDE is slightly larger. Likewise, the PhCH$_2$ radical has a much larger RSE (14.1 kcal mol^{-1}) than that of MeCN (7.6 kcal mol^{-1}),[70] despite having a larger BDE. This is because, in the halides, the R−X bond can be stabilized via resonance with its ionic configuration, R$^+$X$^-$.[71] This effect is larger when R = STY or PhCH$_2$, compared with R = AN or MeCN, because the electron-donating phenyl group helps to stabilize the ionic configuration while the electron-accepting cyano group does not. In a similar manner, the effects of increasing alkylation on the BDEs do not follow expectations on the basis of radical stabilities. For example, the BDEs of the cyano-substituted halides increase in the order MeCN−X < AN−X < IBN−X; STY−X has a higher BDE than PhCH$_2$−X; MA−X and MMA−X have very similar BDEs despite the increased steric hindrance in the latter case. This trend, which we have noted previously for some of these systems,[59,60,72] also reflects the increasing polarity of the R−X bond as hydrogens are replaced with electron-rich methyl groups. Interestingly, once entropic effects are taken into account, the trends reverse as the BDE-lowering effect of increasing steric hindrance with increasing alkylation becomes more important. Nonetheless, with this minor exception, the trends in the free energies largely follow

(70) Krenske, E. H.; Izgorodina, E. I.; Coote, M. L. In *Controlled/Living Radical Polymerization: From Synthesis to Materials*; Matyjaszewski, K., Ed.; ACS Symposium Series *944*; American Chemical Society: Washington, DC, 2006; pp 406–420.
(71) Coote, M. L.; Pross, A.; Radom, L. *Org. Lett.* **2003**, *5*, 4689–4692.
(72) Lin, C. Y.; Coote, M. L.; Petit, A.; Richard, P.; Poli, R.; Matyjaszewski, K. *Macromolecules* **2007**, *40*, 5985–5994.

those in the enthalpies, though the absolute values of the free energies are an average of 9.1 kcal mol^{-1} smaller than the corresponding enthalpies due to the favorable entropic contribution associated with the increased degrees of freedom upon bond breaking.

The effects of solvation on the absolute and relative homolytic BDEs are relatively small. The BDEs in both solvents are slightly higher than the corresponding gas-phase values, by an average of 0.6 kcal mol^{-1} in the case of DMF and 1.0 kcal mol^{-1} in the case of acetonitrile. This probably reflects in part the increased stabilization of the breaking R−X bond, and in part the reduced importance of the increased translational and rotational degrees of freedom upon bond breaking. Overall, we note that, in both the gas and solution phases, the homolytic dissociation is a highly endoergic process, requiring between 34 and 90 kcal mol^{-1} for bond breaking, though the requirement for the active ATRP species is typically to the lower end of this range. It is for this reason that the atom transfer step requires catalysis; the strong halogenophilicity of the Cu(I) catalyst provides the thermodynamic driving force for the reaction and renders the overall reaction much more thermodynamically and kinetically favorable.

It is interesting to compare the experimentally measured values of ATRP equilibrium constants[17] with computed values of free energies of bond homolysis for alkyl bromides and chlorides from the present work. Figure 3 shows the correlation of ΔG values calculated for the free energy of homolytic bond dissociation of alkyl halides in solution with values calculated from the experimental K_{ATRP} values, assuming constant halogenophilicities of Cu(I) complexes (cf. Scheme 4) and taking ethyl 2-bromoisobutyrate (EtiB−Br) and ethyl 2-chloroisobutyrate (EtiB−Cl) as the reference alkyl bromide and chloride, respectively. It can be seen that there is an excellent agreement between theory and experiment, with differences typically within 1 kcal mol^{-1}, in accord with the expected level of accuracy of the corresponding BDEs (see the Supporting Information). This further highlights the predictive power of the theoretical calculations for describing the enormous variations in reactivity of practical ATRP systems.

Heterolytic BDEs and Reduction Potentials. Turning to the heterolytic BDEs (Table 2), we first note that the energetic requirements of this process are smaller than in the homolytic dissociation, requiring free energies in the gas phase that are now negative for all active ATRP species. This is because, as noted above, these values are simply the sum of the corresponding energies for the homolytic dissociations and the reduction of the halogen atom to the halide, and the latter process is highly exothermic. However, it is important to stress that, unlike the homolytic case, the heterolytic bond dissociation reaction is a half-reaction and its overall thermodynamic favorability also depends upon the oxidation potential of the reducing agent with which it is reacting. For the common ATRP catalyst, Cu$^{I/II}$/TPMA, the experimental half-wave value potential is 0.020 V vs SCE in acetonitrile (see Appendix S4 of the Supporting Information). Even for an easily reduced species, such as EtiB−Br (ethyl 2-bromoisobutyrate; SRP$_{dis}$ = −0.42 V vs SCE in acetonitrile, Table 3), this results in an overall dissociative electron-transfer reaction (OSET-C) that is actually endoergic (by 0.44 V or 10.1 kcal mol^{-1} in this example). Due to the high halogenophilicity of the Cu^I/TPMA complex, the first step of the OSET-C reaction is significantly more energetically favorable than the corresponding spontaneous homolytic bond-breaking process (50.36 kcal mol^{-1} in acetonitrile, Table
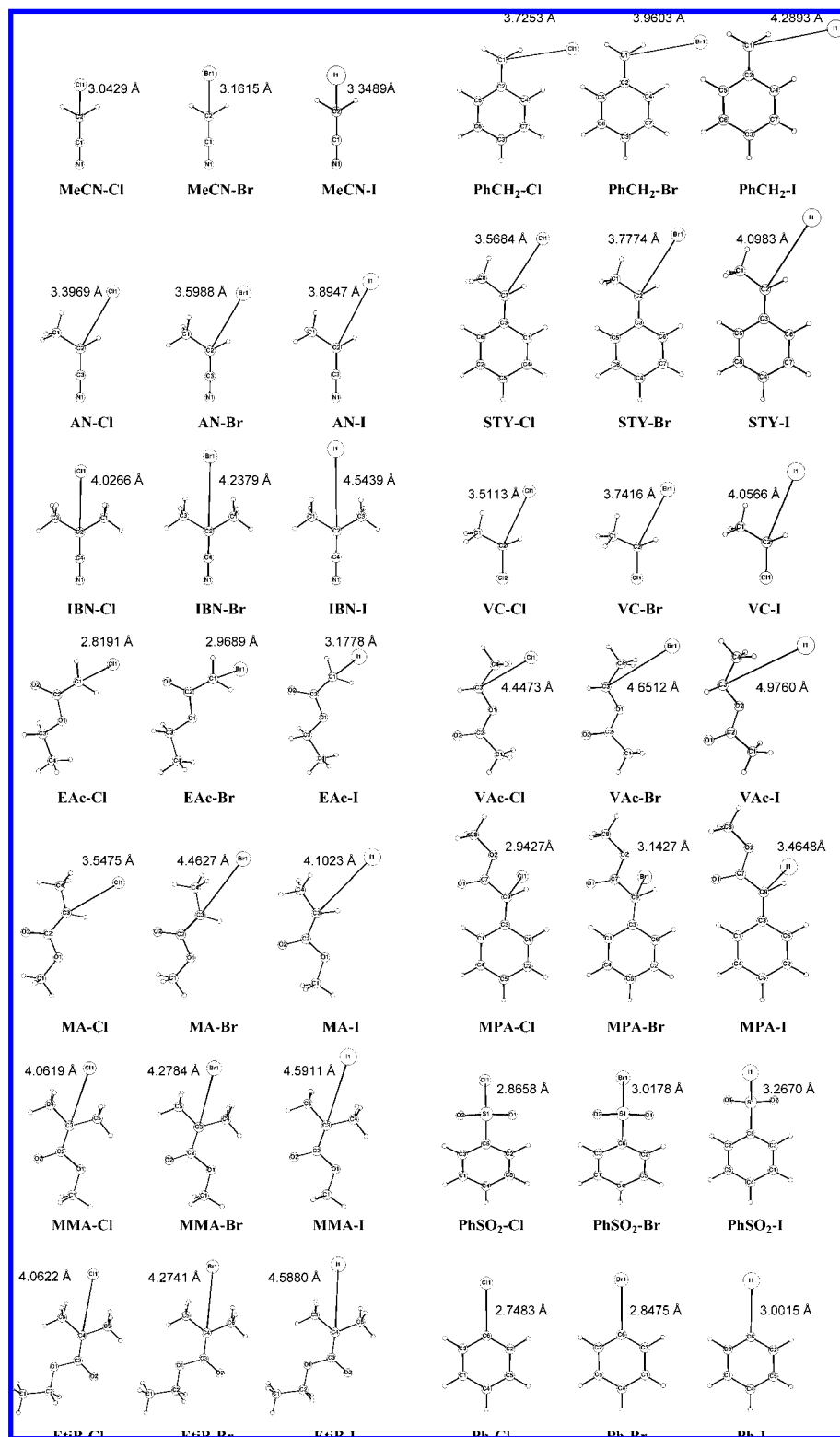
Figure 2. B3LYP/6-31+G(d) optimized geometries of the alkyl halide radical anions in the gas phase.

1) and is energetically similar to the ISET reaction of EtiB−Br with CuBr/CuBr$_2$/TPMA (experimentally measured value, 5.2 kcal mol^{-1} in acetonitrile at 25 °C).[23] Moreover, it must be stressed that, once the halidophilicity of the Cu(II) species is taken into account, the overall thermodynamics of atom transfer are *identical* for the ISET and OSET processes (as indicated in Scheme 2), though their kinetics would of course be very different. On the other hand, if we use the SRP values (Table

3) computed for the adiabatic reduction of RX to RX$^{•-}$, the first step of the OSET-SW mechanism (Scheme 2) for the reaction of Cu$^{I/II}$/TPMA with EtiB−Br in acetonitrile would be endoergic by 0.88 V (20.3 kcal mol^{-1}), which is significantly greater than both the ISET and OSET-C values. Of course, once the subsequent reactions are taken into account, the overall thermodynamic requirements of the OSET-SW mechanism are identical to those of OSET-C and ISET.
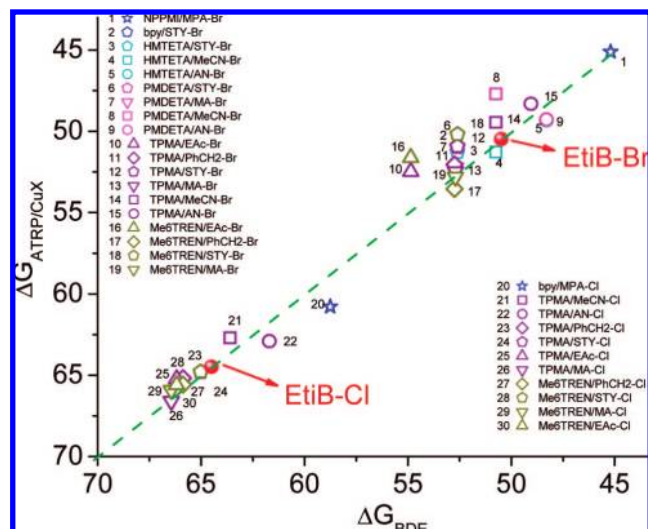
Figure 3. Potential energy surface for dissociation of the RX$^{\bullet-}$ radical anion to R$^{\bullet}$ and X^{-} in the gas and solution phases for AN−Cl, MA−Cl, VAc−Cl, and STY−Cl. Correlation of ΔG calculated from the free energy of homolytic bond dissociation of alkyl halides with experimental values calculated from K_{ATRP} using constant halogenophilicities for various complexes. NPPMI = *N*-(*n*-propyl)pyridylmethanimine, bpy = 2,2′-bipyridine, HMTETA = *N,N,N′,N″,N‴,N‴*-hexamethyltriethylenetetramine, PMDETA = *N,N,N′,N″,N″*-pentamethyldiethylenetriamine, TPMA = tri(2-pyridylmethyl)amine, Me$_6$TREN = tris(2-(dimethylamino)ethyl)amine.

Thus, on a thermodynamic basis, the ISET and OSET-C processes should give the same final products and cannot be distinguished. Fortunately, Marcus theory for electron-transfer processes allows us to estimate the activation energy of the OSET-C process and to compare this rate constant with the experimentally observed one. The results of such a comparison for bromoacetonitrile with CuBr/TPMA in acetonitrile will be presented in a subsequent section.

Not surprisingly, the effects of solvation on the heterolytic BDEs are much larger than in the uncatalyzed homolytic BDEs; this is because the halide anion that is produced by this reaction is much more heavily stabilized by the solvent than the corresponding halogen radical that results from the uncatalyzed homolytic reactions. This effect is significant, with both solvents lowering the heterolytic alkyl halides BDEs by an average of 62.6 kcal mol^{-1}, compared with the gas-phase values. As in the case of the homolytic BDEs, the heterolytic BDEs are lowest for the iodides and highest for the chlorides; however, the differences are now much smaller, particularly in solution. For a given alkyl group and copper catalyst, the thermodynamic favorability of the heterolytic bond dissociation process, relative to the uncatalyzed homolytic BDE, increases from iodine to bromine to chlorine due to the increasing reduction potential of the halogen atom. Within each series of halides, the trends in the BDEs are of course identical to those in the homolytic BDEs, as the reactions differ only in the nature of halide/halogen product.

The adiabatic EAs and SRPs of the alkyl halides show trends similar to those of the corresponding heterolytic bond dissociation reactions, and the adiabatic and dissociative values show a reasonable degree of correlation with one another ($R^2 = 0.95$). As noted above, in the gas phase, the alkyl halides rearrange upon accepting an electron to form stable complexes between the alkyl radical and the halide. Thus, the alkyl halide "radical anions" are already largely dissociated and are thus subject to

stereoelectronic influences similar to the fully dissociated species (see Figure 2).

The stability of the alkyl halide radical anion complexes toward complete dissociation can be assessed by comparing the adiabatic and dissociative values of their EAs and SRPs. In the gas phase, the adiabatic EA is higher than the dissociative value by approximately 0.5 eV, and hence the complexes are relatively stable. In the solution phase, we find that the complexes are not stable to dissociation, and this is also evident in the fact that the "adiabatic" SRPs, as calculated using the gas-phase geometries of the optimized alkyl halide radical anions, are an average of 0.38 V (8.7 kcal mol^{-1}) more negative than the dissociative values, though the energy difference varies somewhat according to the substituents. Thus, in all cases, our calculations predict that, on a thermodynamic basis at least, electron transfer to an alkyl halide in solution results in dissociation to the corresponding alkyl radical and halide anion.

To examine the stability of the alkyl halide radical anions further, we calculated the potential energy surfaces associated with the dissociation of the RX$^{\bullet-}$ radical anions into R$^{\bullet}$ and X^{-}. These were obtained as relaxed scans along the bond length between the terminal carbon and the halogen atom. Optimizations were carried out in both the gas and solution phases, and all energies were then improved to our high level of theory, G3(MP2)-RAD(+). To check for the importance of multiref-erence effects, we calculated the T1 diagnostic along the dissociation pathway for the case of MA-Cl. In the vicinity of the ion−radical complex (i.e., at alkyl halide distances >3 Å), values less than 0.02 were obtained in all cases, confirming the suitability of the single-reference method. Solvation energies were obtained using both the CPCM model, as used to obtain the SRPs, and also a more advanced model, COSMO-RS.[67] Results for four typical examples, AN−Cl, VAc−Cl, MA−Cl, and STY−Cl, are provided in Figure 4.

From Figure 4, we can see that there is a weak complex between R$^{\bullet}$ and X^{-} with a large separation (3−4 Å) in the gas-phase calculation for all species, and all separated species have higher energies than those of the complex. However, in solution, while there is also a weak complex, its energy is much higher (0.4−0.6 eV mol^{-1} or 9.2−13.8 kcal mol^{-1}) than that of the separated species. The use of the improved solvation model, COSMO-RS, makes little difference to the overall thermochem-istry of the reduction process (<1 kcal mol^{-1}) but does emphasize the dissociation barrier slightly at larger separations (6−8 Å). Nonetheless, even using the more sophisticated solvation model, the calculated barrier to separation is very small (<0.1V), close to the estimated error in the calculations themselves and much less than the energy released upon dissociation. Moreover, the minima associated with the com-plexes are broad, and the dissociation barriers tend to occur at large radical−ion distances (as much as 6−8 Å). Thus, even using the more sophisticated treatment, the data indicate that the radical−anion pairs formed by the reduction of alkyl halides are at best short-lived intermediates that undergo rapid dis-sociation. Hence, in solution, OSET does occur via concerted dissociative electron transfer involving in-cage ion−dipole interactions if polar groups are present in the radical, according to the "sticky model".[37]

Reduction Potentials of Alkyl Radicals. Under the OSET mechanism, the ATRP catalyst reduces the alkyl halide, resulting in its dissociation to the alkyl radical and halide anion (OSET-C). Under such a reducing environment, it is possible that the propagating alkyl radicals produced by this reaction could also
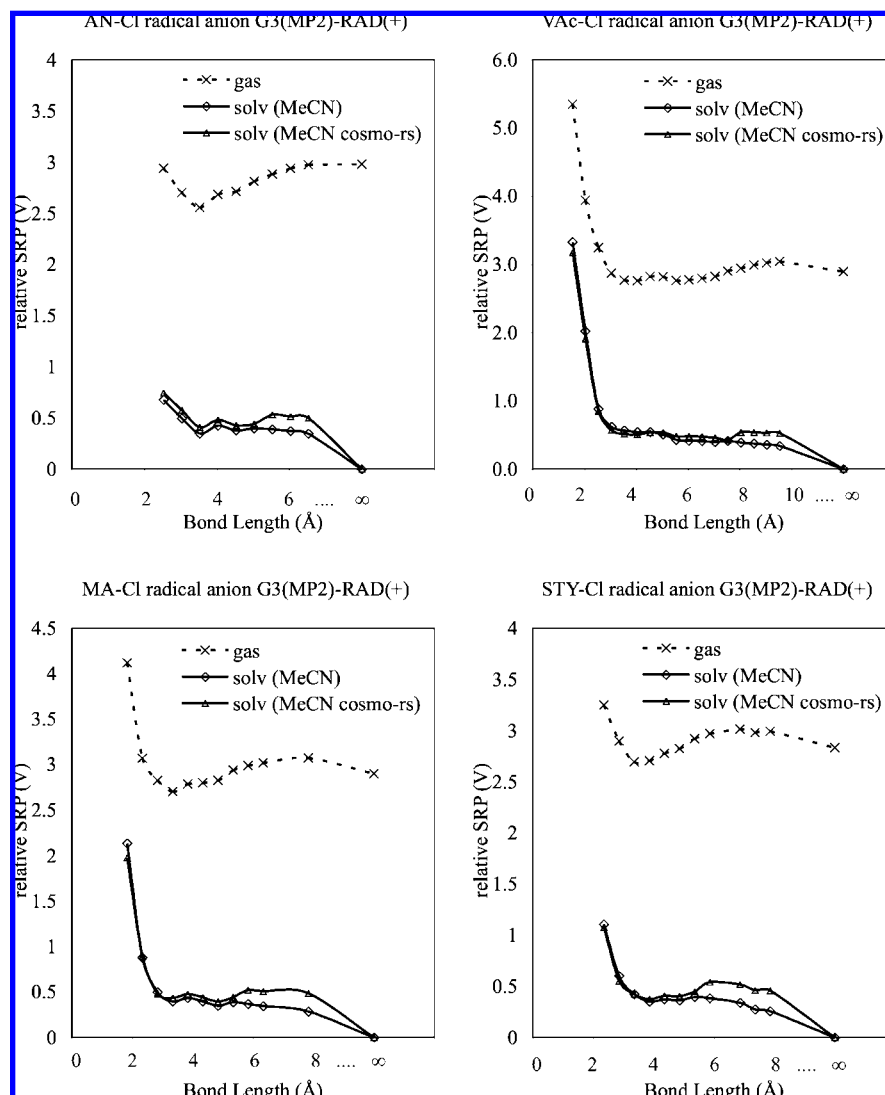
Figure 4. Potential energy surface for dissociation of the RX$^{\bullet-}$ radical anion to R$^{\bullet}$ and X^{-} in the gas and solution phases for AN−Cl, MA−Cl, VAc−Cl, and STY−Cl.

undergo reduction to the corresponding carbanions (Scheme 3) and terminate chain growth by proton abstraction from solvent or protic impurities. To assess this possibility, the gas-phase EAs and corresponding SRPs of the alkyl radicals, together with the halogens and PhSO$_2$, are shown in Table 4. If we compare these SRPs with those for dissociative reduction of the corresponding alkyl halides (Table 3), we note that the trends are quite different. To some extent this is not unexpected: when the alkyl radicals are reduced, the alkyl radicals are the reactants, whereas in dissociative reduction of the alkyl halides, the same species are the products. Thus, in the first case, substituents that stabilize a radical disfavor its reduction, and in the latter case they favor reduction of the alkyl halide. Thus, for example, STY−X and PhCH$_2$−X are relatively easy to reduce, whereas STY and PhCH$_2$ radicals are not. However, these trends are complicated by the fact that electron-withdrawing groups such as CN and COOCH$_3$ favor reduction of *both* the alkyl radicals (by stabilizing the carbanion products) and alkyl halides (by weakening the alkyl halide bond). As a result of these competing influences, the species bearing radical-stabilizing and/or electron-donating groups (such as PhCH$_2$, STY, VC, and VAc) tend to have lower reduction potentials than their corresponding halides, while species that are not stable as radicals (such as Ph) or do

bear electron-withdrawing groups (such as MeCN, EAc, PhSO$_2$) have reduction potentials that are higher.

The implication of these results is that, for the species such as the MeCN, EAc, PhSO$_2$, and Ph radicals, any catalyst capable of reducing the alkyl halide is also likely (thermodynamically) to reduce the alkyl species to anions and lead to chain-breaking side reactions. This effect is likely to be particularly relevant when alkyl chlorides are used as the dormant species, as these have stronger alkyl halide bonds and thus lower reduction potentials. Indeed, for such monomers (or initiators), less reducing catalysts are required in practice; better control is also attained at lower catalyst concentration.[46,47,73]

Kinetic Comparison of ISET and OSET for the Case Study, Bromoacetonitrile with Cu^I/TPMA. In the present work, our ab initio calculations have focused on the electrochemical and thermochemical aspects of the reaction mechanism. Discrimination between the ISET and OSET pathways, however, also requires a consideration of the transition structures associated with respective pathways. Unfortunately, ab initio calcula-

(73) Matyjaszewski, K.; Tsarevsky, N. V.; Braunecker, W. A.; Dong, H.; Huang, J.; Jakubowski, W.; Kwak, Y.; Nicolay, R.; Tang, W.; Yoon, J. A. *Macromolecules* **2007**, *40*, 7795−7806.

tions of such species, involving as they do large transition-metal complexes in solution, cannot as yet be performed with the same level of accuracy as the calculations of small organic molecules presented herein. Fortunately, the barriers for the OSET process can be estimated using the well-known Marcus theory for outer-sphere electron-transfer reactions, provided the relevant electrochemical and thermodynamic parameters are known. These can then be compared with the experimentally determined reaction barriers for the ATRP process, so as to establish whether the reaction occurs via OSET or ISET.

As described in Appendix S2 (see Supporting Information), we compared the kinetics of both ISET and the concerted OSET processes for the case study of bromoacetonitrile with $Cu^{I/II}$/TPMA in acetonitrile at 25 °C. The outer-sphere ET reaction,

$$[Cu^I(TPMA)]^+ + MeCN\text{-}Br \xrightarrow{k_{OSET}} [Cu^{II}(TPMA)]^{2+} +$$
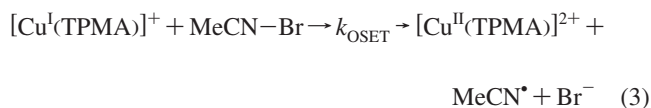
$$MeCN^{\bullet} + Br^- \quad (3)$$

involves a concerted DET to MeCN-Br, as is well established in the literature.[37] According to Marcus theory, the rate constant can be calculated by eqs 4 and 5,

$$k_{ET} = Z_{12} \exp\left(-\frac{\Delta G_{12}^{\ddagger}}{RT}\right) \quad (4)$$

$$\Delta G_{12}^{\ddagger} = \Delta G_{0_{12}}^{\ddagger}\left(1 + \frac{\Delta_r G^{\circ}}{4\Delta G_{0_{12}}^{\ddagger}}\right)^2 \quad (5)$$

where $\Delta G_{0_{12}}^{\ddagger}$ is the intrinsic barrier of the reaction (which is an average value of the energy barrier for the self-exchange reaction between $Cu^I(TPMA)/Cu^{II}(TPMA)$, $\Delta G_{0_{11}}^{\ddagger}$, and self-exchange for MeCN-Br/MeCN$^{\bullet}$,Br$^-$, $\Delta G_{0_{22}}^{\ddagger}$) and $\Delta_r G^{\circ}$ is the reaction free energy: $\Delta_r G^{\circ} = -F(E_{MeCN\text{-}Br}^{\circ} - E_{Cu(II)/Cu(I)}^{\circ})$. Unfortunately, not all the data required for estimating the frequency factor Z_{12} and $\Delta G_{0_{12}}^{\ddagger}$ are available. Thus we introduced the following approximations: the self-exchange ET rate constant for [Cu-(TPMA)]$^{2+/+}$ was assumed to be similar to that of [Cu-(dpm)$_2$]$^{2+/+}$; the radius of the complex was derived from crystallographic data for the CuCl(TPMA); and since the concerted DET is kinetically favored by the sticky contribution, we lowered the intrinsic barrier by the same quantity experimentally determined in DMF, as the radical–anion interactions depend on the dielectric constants which are very similar for the two solvents. As we show in the Supporting Information, the effect of these approximations on the accuracy of the results is several orders of magnitude smaller than the difference between the calculated OSET-C and experimental ISET rates, and therefore they do not affect the conclusions. The resulting estimated value of the activation free energy for the OSET-C is 26.8 kcal/mol and $k_{OSET} = 6 \times 10^{-9}$ M^{-1} s^{-1}.

The reaction free energy for OSET-C was calculated using the SRPs reported in Table 3 for the dissociative reduction of MeCN-Br (−0.46 V) and the experimental reduction potential of [Cu(TPMA)]$^{2+/+}$ (0.015 V vs SCE; see Appendix S4 of the Supporting Information), whereas the intrinsic barrier was calculated from the estimated self-exchange intrinsic barriers or from the solvent reorganization energy and C-Br BDE for MeCN-Br reported in Table 1 ($\Delta H = 58.86$ kcal mol^{-1}). The reaction free energy for ISET was determined by K_{ATRP} reported in literature[23] ($K_{ATRP} = 5.6 \times 10^{-5}$), whereas the activation free energy was derived from the corresponding experimental k_{act} value ($k_{act} = 82$ M^{-1} s^{-1}).[22]

In order to reach the same products in OSET and ISET processes, one more step has to be considered in the OSET

mechanism, i.e., the association of bromide anion with [Cu-(TPMA)]$^{2+}$ species. The equilibrium constants for this process (halidophilicity) were determined for various copper complexes,[36] and they range from $K = 10^4$ to 10^6 M^{-1}, which leads to $\Delta_r G^{\circ} \approx -6$ kcal mol^{-1}. This results in an overall free energy change for the OSET-C process of 5 kcal mol^{-1}, which is very similar to the experimental[23] value of 5.8 kcal mol^{-1}. In principle these two values should be identical—the fact they differ by only 0.8 kcal mol^{-1} further confirms the accuracy of the experimental and ab initio data used in the calculations and the validity of the approximations made. Since the activation free energy for this reaction is quite small (∼5 kcal mol^{-1}), it has no kinetic effect on the overall OSET process, which is kinetically controlled by the concerted dissociative ET to MeCN-Br. Indeed, this step has a very high activation free energy owing to the contribution of the breaking carbon–bromine bond. The overall free energy change in the OSET process can be also evaluated by comparing the SRP of MeCN-Br (−0.46 V, Table 3) with the SRP of Cu^{I}Br(TPMA)/Cu^{II}Br$_2$(TPMA), which is −0.24 V.[48] These values give $\Delta G^{\circ} = 5.1$ kcal mol^{-1}, again in a very good agreement with experimental values.

Figure 5 compares the energy profiles associated with the ISET and OSET-C processes. From these results it is clear that, for the present case study at least, the activation free energy of the ISET mechanism (13 kcal mol^{-1}) is 14 kcal mol^{-1} lower than that of the OSET process, while the rate constant of the former mechanism ($k_{act} = 82$ M^{-1} s^{-1}) is ∼10^{11} times higher than that of the latter, even in the more favored sticky pathway. As we show in the Supporting Information, this difference is much greater than any approximations in the analysis or errors in the computational and/or experimental data, which would affect the results by no more than 1−2 orders of magnitude. Moreover, if the sticky contribution is not considered, i.e., in the case of the normal dissociative mechanism, the activation energy becomes a further 3 kcal mol^{-1} higher and the rate constant a further 100 times lower. To reach the same rate constant for OSET-C mechanism, the reducing complex should have a SRP < −1.24 V, but this would have a catastrophic effect on the reduction of the MeCN radical, which would be enormously fast under those conditions.

Mechanistic Implications. On the basis of the thermochemical calculations presented herein, we can now draw some conclusions about the mechanism of ATRP.

First, the results obtained show that solvation has a crucial effect on the free energies of the processes of reduction of alkyl halides. In fact, while the solvent has only a small effect on the homolytic bond dissociation, it influences strongly the heterolytic one, as illustrated by the data reported in Table 2. Thus, considerations based only on energies related to the gas phase are meaningless for processes occurring in solution.

Second, our studies of the radical anions produced via electron transfer to the alkyl halides indicate that the latter, upon receiving an electron, undergo significant rearrangements to form complexes between the halide anion and alkyl radical. These complexes, which are not true radical anions, appear to be relatively stable in the gas phase thanks to important dipole–anion interactions, especially when the radical possesses a significant dipole moment. In such cases, dissociative electron transfer could, in principle, proceed in the gas phase via a two-step process (OSET-SW), even if this is quite different from the mechanism proposed by Guliashvili and Percec,[41] since no true radical anions are formed. In any case, once solvent effects are taken into account, we find that these complexes are not
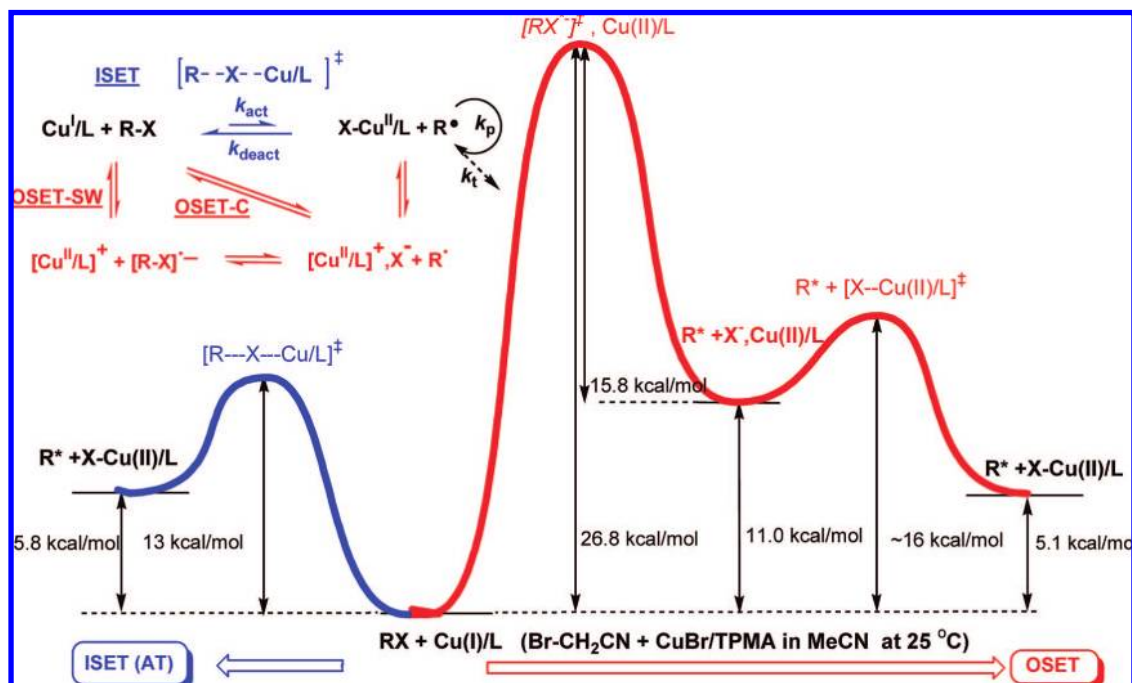
Figure 5. Comparison of free energies during ISET and concerted OSET processes for the reaction of bromoacetonitrile with Cu^I/TPMA in acetonitrile at 25 °C.

stable to dissociation; thus, in a practical experimental setup, OSET is predicted to occur via concerted dissociative electron transfer (Scheme 6), i.e., by the OSET-C mechanism. An important implication of this is that, if concerted dissociative electron transfer does occur, the reverse process (which is termolecular) would be predicted to occur with a very slow rate.

Third, we note that, while there is considerable variation among the species examined, the energetic requirements for the homolytic bond dissociation process are very large for all of the alkyl halides examined. This implies that, if the homolytic dissociation occurs in practice, it must occur via a (catalyzed) concerted mechanism (i.e., ISET) rather than the hypothetical stepwise process depicted in Scheme 4. As expected, the homolytic dissociation process is favored by substituents capable of stabilizing the product alkyl radical and/or by electron-withdrawing substituents and is most favored for the iodides and least favored for the chlorides. In practical terms, this means that monomers bearing electron-withdrawing groups and/or radical-stabilizing groups such as acrylonitrile and styrene require less active ATRP catalysts than monomers such as vinyl chloride and vinyl acetate. On the basis of the homolytic BDEs, one might also assume that alkyl iodides and bromides should require less active catalysts than the chlorides. However, it must be remembered that the overall thermodynamics of the atom-transfer reaction depends strongly on relative halogenophilicities of transition-metal complexes. Since the Cu^{II}—I bond is much weaker than Cu^{II}—Br, and considerably weaker than the Cu^{II}—Cl bond, the differences in the ATRP equilibrium constants of the alkyl chlorides, bromides, and iodides are not very large.

Fourth, while the heterolytic bond dissociation of alkyl halides is highly exoergic (particularly in solution), this is a half-reaction, and its overall thermodynamic feasibility also depends upon the oxidation potential of the reducing agent. In the case of the very active ATRP catalyst, Cu$^{I/II}$/TPMA, the overall heterolytic bond dissociation reaction is also endoergic for all of the species studied. Although this first step in the OSET process was found to be considerably more thermodynamically

favorable than the uncatalyzed homolytic dissociation, when compared with the concerted ISET process for a typical example (MeCN—Br with Cu$^{I/II}$/TPMA), its thermodynamic requirements were found to be very similar, in the case of the OSET-C mechanism (see Scheme 2). In other words, on a thermodynamic basis, both concerted ISET and OSET-C appear to be feasible. In any case, the OSET-SW mechanism is an unfavorable pathway with respect to both ISET and OSET-C.

Fifth, even though the thermodynamics of ISET and OSET-C must be the same (since the initial and final states are the same), we found that the kinetics are very different, as clearly demonstrated by the case study of bromoacetonitrile with Cu/TPMA. In effect, the endoergic OSET mechanism is not possible, since it would have an intrinsic barrier greater than 27 kcal mol^{-1} and, consequently, a rate constant lower than 10^{-11} M^{-1} s^{-1}. Only the ISET mechanism can explain the much higher experimental rate constants which are recorded for many endoergic reductions of alkyl halides by effective ATRP catalysts. This is a wonderful serendipity since our electrochemical calculations suggest that OSET-C is not likely to be successful for monomers (such as acrylates) that bear electron-withdrawing groups but do not have highly stabilized propagating radicals. For, in those problematic cases, the one-electron reduction of the propagating radical is predicted to be more thermodynamically favorable than the one-electron reduction of the corresponding alkyl halide; furthermore, it surely is more kinetically favored, since the intrinsic barrier is much lower than that for the alkyl halide reduction. Thus, catalysts with reducing potentials sufficient to enable reduction of the alkyl halides, i.e., with a SRP more negative than the halide, would also reduce the propagating radicals, resulting in catastrophic chain-breaking side reactions.

Finally, the choice of appropriate catalyst for LRP must take into account the thermodynamic requirements and, particularly, the redox properties of the dormant halide and the propagating radical, to avoid chain-breaking reactions due to the reduction of the last. Since ISET is the preferred pathway for preventing

this side reaction, halido-/halogenophilicity of the catalyst seems to play a crucial role.

Supporting Information Available: Complete ref 54 (Appendix S1); full description of the Marcus theory calculations (Appendix S2); evaluation of the accuracy of the theoretical data (Appendix S3); details of the experimental determination of the reduction potential for Cu(TPMA) complexes (Appendix S4); homolytic (Table S1) and heterolytic BDEs (Table S2) at various levels of theory and experiment for all alkyl halides studied; theoretical and experimental values of the EAs and SRPs (Table S3) for selected species; theoretical and experimental homolytic BDEs in acetonitrile at 22 °C (Table S4); B3-LYP/6-31+G(d) optimized geometries of all species in the gas phase (Table S5); and UHF/6-31+G(d) optimized geometries of all species in dimethylformamide (Table S6) and acetonitrile (Table S7). This material is available free of charge via the Internet at http://pubs.acs.org.

JA8038823